



NLR-TP-2005-224

Aeroelastic CFD studies for geometrically complex aircraft configurations

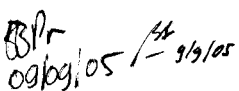
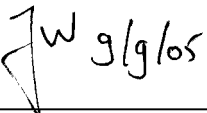
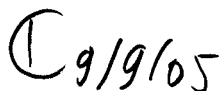
J.W. van der Burg, B.B. Prananta and B.I Soemarwoto

This report has been based on a paper presented at the International Forum on Aeroelasticity and Structural Dynamics (IFASD2005), Munich, Germany, July, 2005.

This report may be cited on condition that full credit is given to NLR and the authors.

Customer: National Aerospace Laboratory NLR
Working Plan number: AV.1.E/AV.1.F
Owner: National Aerospace Laboratory NLR
Division: Aerospace Vehicles
Distribution: Unlimited
Classification title: Unclassified
June 2005

Approved by:

Author	Reviewer	Managing department
 09/09/05 / 9/9/05	 9/9/05	 9/9/05



Summary

The paper reports aeroelastic CFD studies conducted for a civil and military aircraft configuration. An aeroelastic method for geometrically complex configurations consisting of multiple components (like flap, slat, pods, weapons etc.) has been developed and deployed to examine aeroelastic behaviour of a high-lift wing. The aeroelastic method has been verified for a generic fighter.



Contents

List of Symbols	5
1 Introduction	7
2 Research on high lift wing deformation	9
2.1 Definition of a structural model	9
2.2 Aeroelastic analysis of a high-lift wing	10
3 Aeroelastic analysis of a generic fighter aircraft	11
4 Conclusions	13
5 References	14

(23 pages in total)



List of Symbols

α	angle of attack
C_L	Lift coefficient
dx, dy, dz	Displacements in co-ordinate directions
g	gravity
l_{ref}	Reference length aerodynamic grid
l_{str}	Reference length (structure)
M_∞	Mach number at infinity
n_z	Load factor
q_∞	Dynamic pressure
Re	Reynolds number
S_{aero}	Reference area of the aerodynamic grid
S_{str}	Reference area of the structural grid
x, y, z	Physical co-ordinates



This page is intentionally left blank.



1 Introduction

Currently aircraft industry is heavily investing in development of new all-composite aircraft. Boeing has committed itself to produce the 7E7 Dreamliner (Ref. [6]) and Airbus is currently developing in response the A350 aircraft (Ref. [5]). In large parts of the fuselage, wing and tail composite materials will be introduced.

Stork Aerospace is involved in the design and production of moving parts of the wing for the Dassault Falcon 7X using light weight materials (Ref. [2]). Composite structure is a good substitute for metals in aircraft construction when high strength-to-weight and/or stiffness-to-weight ratios are required (Ref. [6]).

However, the aeroelastic implications in introducing an all-composite fuselage and wing structures have to be carefully investigated especially for high-lift wings. High-lift wing deformation will typically occur at take-off and/or landing due to the high loading needed to generate the necessary lift (an example for a commercial aircraft is shown in Figure 1). Due to differences in stiffness and weight, for instance compared to the traditional aluminium wing structures, the aeroelastics characteristics are changed. The trend in high-lift system designs is towards high-lift systems with a reduced structural and mechanical complexity compared to more traditional high-lift systems. Control surfaces should be designed for limit loads resulting from flight manoeuvring conditions (including pilot effort). This means that hinge loads due to control surface deflection need to be verified in order to meet JAR requirements.

Due to the appearance of aeroelastic effects it can be expected that the airframe noise characteristics are altered. It is known that aircraft are at their 'loudest' when landing gear, wing flaps, and slats (see Figure 1) are deployed, see Ref. [10]. Introduction of new engine technologies have generated significant noise reduction. As a result of this the airframe noise component, including flap/slat gap noise and landing gear noise, has become relatively more important in particular for the landing condition. For high lift devices, less noise reduction has been achieved mainly due to more complex integration constraints. Both the EU vision 2020 statement and the NASA vision 2050 target reduction of airport noise levels. In Ref. [9] it has been concluded that: "Airframe noise reduction is becoming increasingly important".

Many innovative solutions, reducing weight, reducing complexity, achieving noise reduction or increasing high-lift performance have been proposed. For instance for military aircraft like the F-111 and F-15 the gaps between wing and control surfaces have been faired using highly flexible structures which allow a continuous mould line (Ref. [1]). Furthermore, high-lift efficiency improvements have been proposed by introducing for instance advanced flow control



devices (see Ref. [8]), quote from Ref. [7]: “We’ve also demonstrated advanced aerodynamics flow control techniques that would allow highly efficient and simpler vehicle controls and high-lift systems”. In order to employ these improvements the aeroelastic effects should be accounted for.

Surprisingly, there is as yet still not sufficient insight into the flow physics of a high-lift configuration to improve high-lift characteristics. Nevertheless, aircraft are taking-off and landing on a routine basis. Quote from Ref. [3]: “Even for these vehicle systems, there are many flow phenomena, especially at the edges of the flight envelope such as buffet and take-off and landing that are not well understood”. Since, for high-lift flow the presence of geometrical detailed components, like flap track fairings and slat tracks, have a significant influence (see Ref. [4]), it is essential that local aeroelastic effects are modelled as well. In classical aeroelastic approaches typically a global interpolation method is adopted in order to relate the aerodynamic forces to the structure of the aircraft. This global method cannot be satisfactorily employed for a multi-component aircraft configuration, like a take-off or landing configuration.

In this paper experiences with an aeroelastic method¹ are presented which is capable of modelling aeroelastic effects for geometrical complex aircraft configurations with multiple components. The need for an aeroelastic tool capable of handling geometrically complex configurations with multiple components has been identified in many occasions, e.g. when analysing either the static aeroelastic (determination of loads) or dynamic aeroelastic (studying stability) behaviour of a fighter aircraft (see Figure 2) with various types of stores mounted, or for innovative high-lift wing concepts.

At NLR, thusfar, aeroelastic analyses requiring advanced flow modelling have been conducted by employing an aeroelastic method based on a multi-block structured grid approach.

Experience with this method has learned that the turnaround time of the multi-block based method is prohibitively large for a geometrically complex configuration and a common way to encompass this, is by an intelligent judgement of geometry simplification.

For example, in case of fighter aircraft stores the aerodynamic forces working at the stores are neglected, but the inertia forces working on the stores are retained. Important drawback here is, however, that when a new configuration has to be analysed the aerodynamic forces may become significant.

¹ Fluid-structure coupling methodologies involving unstructured grid technology have been developed and researched in the framework of the EU Taurus project (Ref.[11]).



In the paper an example of the developed aeroelastic method for multiple components will be presented. A static aeroelastic study has been conducted for the KH3Y wind tunnel model (which is a representation of an Airbus-type high-lift wing) under ETW wind tunnel conditions. Furthermore, the static aeroelastic behaviour has been verified for a generic fighter aircraft.

2 Research on high lift wing deformation

An aeroelastic study has been conducted to assess the deformation of a multi-component high-lift wing². To this purpose a high-lift wing test case has been selected that represents the KH3Y high-lift wind tunnel model in the ETW. Model deformation is experienced in ETW due to the necessary high loading q_∞ to realise the highest Reynolds numbers. It is expected that by taking the aeroelastic deformation of the high-lift wing into account, a better agreement with the experimental lift curve will be achieved.

2.1 Definition of a structural model

In order to withstand the high pressure loadings in the ETW, the high-lift wind tunnel model is made out of ASTM 579 steel. The wind tunnel model is not solid due to presence of wind tunnel equipment. Inside the main wing, room has been created to allow for the installation of instrumentation like for instance the pressure tubes. To withstand cryogenic conditions in the ETW tests all metal parts of the model have been made from the same material.

The structural model has been derived from the CAD geometry definition of the wind tunnel model, which is defined in terms of IGES patches (for flap, main wing and slat). The CFD geometry of the high-lift wing is shown in Figure 3.

In the construction of the structural model of the high-lift wing a number of approximations have been made. Firstly, it has been assumed that the fuselage will not be aeroelastically deformed. A structural model has been created for the wing elements only. This structural model is based on the geometrical data of 20 wing sections (see also Figure 3). The wing is assumed to be solid, so that the interior rooms are not modelled.

The slat is modelled by means of beam elements. Since a beam element does not represent the cross-section of a slat very well, this approximation may be due for further improvement by adopting other means of structural elements. Slat tracks and flat track fairings are made of an aluminium alloy and have been modelled by means of beam elements. At the location of the

² This work forms part of the Eurolift II project (Ref.[12]). To distinguish between these geometry effects an in-depth CFD study will be carried out in the Eurolift II project that focuses separately on the influence of: model deformation, presence of wind tunnel walls, presence of the peniche and the installation of slat tracks.



(slat and flap) tracks the structural grid nodes of the main wing and associated flap or slat node are connected, so that they have the same degree of freedom. The final structural model is shown in Figure 4.

Verification tests have been conducted to check the validity of the structural grid. Application of a linear mode shape, a pressure force at the wing tip and a torsion of the high-lift wing have been verified. No appropriate test bench data are yet available in order to validate the structural model.

2.2 Aeroelastic analysis of a high-lift wing

A static aeroelastic analysis for a high-lift wing with flap track fairings installed has been conducted for an angle of attack of $\alpha=12$ degrees at Mach-number $M_\infty=0.2$ and free stream dynamic pressure $q_\infty=6.5$ kPa. This angle of attack represents a point in the linear range of the lift curve. In the aerodynamic grid the slat tracks have not been modelled (the slat tracks are represented in the structural model). Viscous flow is assumed and a hybrid (prismatic-tetrahedral) grid having 4 million nodes has been adopted in the aeroelastic computation (20 prismatic layers and approximately 120000 nodes on the aerodynamic surface). A grid coarsening factor of 4 has been employed in spanwise direction at the leading edges of the flap, slat and main wing. The unstructured surface grid is shown in Figure 5.

The aeroelastic simulation is performed using an iterative algorithm consisting of three steps:

- (i) The flow analysis using the unstructured flow solver which provides the pressure on the surface,
- (ii) The structural analysis providing the surface force distribution and its corresponding surface deformation, and
- (iii) The grid deformation procedure that gives a new unstructured grid for the next iteration.

In the aeroelastic computation 10 deformations steps have been taken in total to converge the maximum deformation. The convergence history of the aeroelastic computation is shown in Figure 6. The upward dimensionless displacement in z-direction is in the order of $0.03 l_{ref}$.

A view of the final computed deformed high-lift wing is shown in Figure 7. As expected, for the high-lift swept wing a global bending combined with torsion has been obtained. The torsion of the high-lift wing locally reduces the angles of incidence at the outboard part of the wing. In addition, also more local aeroelastic effects are present. From the contour lines of constant deformation it can be observed that the deformation of the outboard flap and slat differ from the deformation of the main wing. On the inboard side the flap is attached to the fuselage. It can be observed that the aeroelastic deformation has a local effect on the flap at this location. In an

aero-elastic study based on inviscid flow conducted for a high-lift configuration without the flap track fairings installed a similar aero-elastic behaviour has been found.

The change in flap-gap and slat-gap height becomes clear in Figure 8 where a cross-section of the high-lift wing is shown for the rigid and the deformed wing at the outboard section of the high-lift wing. It can be seen that the flap gap height has increased at this station.

In Figure 9 the smallest heights between the flap and main wing and the slat and main wing are shown as a function of wing span for the rigid and deformed wing. As expected at the location of the flap tracks the change in flap-gap height equals zero, whereas in-between and outside the flap tracks differences are observed. The flap-gap height is reduced approximately with 10% between the third and fourth flap track, and with 20% between the fourth and fifth flap track. In contrast, the slat gap height has been increased in between the slat tracks. The slat-gap is not altered at the location of the slat tracks (note that the slat tracks are only modelled in the structural model).

The aeroelastic method did run automatically on a single processor of the NEC SX5 supercomputer. In order to compute the first flow solution 2400 iterations have been taken to converge the lift coefficient. The total cpu-time for the first flow solution is 28 hours. One aeroelastic step in the aeroelastic loop amounts to 6.5 cpu-hours except for the first aeroelastic loop which takes 7.5 cpu hours in order to compute the transformation matrix needed to interpolate the aerodynamic and structural grid.

Reductions in turnarounds time are certainly feasible. A reduction with a factor 2 is possible in case algorithms in the aeroelastic loop that do not vectorise, are executed on a scalar machine. For a Silicon Graphics Workstation this would result in a cpu-time of 3 hours for the aeroelastic loop. Operation in parallel mode is possible for the fluid-structure coupling, but has not been attempted for this case.

3 Aeroelastic analysis of a generic fighter aircraft

Static deformation of an F-16 fighter at various flight conditions and various store configurations have been investigated at NASA Dryden and are presented in (Ref. [13]). One of the NASA Dryden static deformation test cases has been selected for method validation. The test case is a generic F-16 configuration equipped with an advanced medium range air to air missile (AMRAAM) at the wing tip during a 5-g symmetrical pull-up manoeuvre at an altitude of 5.000 feet with a running engine. A static aeroelastic free-free simulation has been conducted using a simplified structural model of the F-16 configuration with about 100 degrees of



freedom, see Figure 10. The reference length of the structural grid is $l_{str}=135.84$ inch and with reference area $S_{str} = 21600$ inch².

A multi-block unstructured aerodynamic grid, see Figure 10, has been created for the semi-span configuration of an F-16. To illustrate multi-block unstructured grid technology the unstructured grid has been built in two steps, the first step is the creation of an internal tetrahedral grid close to the aerodynamic surface and the second step is the creation of a tetrahedral grid for the far field which is merged with the internal grid. Multi-block unstructured technology introduces more flexibility in the unstructured grid generation process.

The grid spacing has been specified by means of source terms at leading and trailing edges of the wing, the horizontal stabilizer and the tail. The final tetrahedral grid contains approximately 1.5 million nodes in the three-dimensional grid with 236000 nodes on the aerodynamic surface. The reference length of the aerodynamic grid is $l_{ref} = 3.45$ m and the reference area is $S_{aero} = 13.9$ m².

To match the g-level during the free flight simulation the aircraft needs to be trimmed. The trimming has been carried out by modifying the angle of attack and the control surface deflection in such a way that all forces and moments on the aircraft are in balance. The engine is operational (engine inflow and outflow is modelled) and a symmetrical flow condition is considered. The necessary lift coefficient to produce the g-level is $C_L=0.385$. In total 200 multigrid 5-level W-cycles have been taken to achieve the fixed lift condition. A second order upwind scheme and a 3-stage time-integration algorithm have been adopted to advance the flow solution in time.

In the static aeroelastic computation 6 fluid-structure-coupling iterations have been taken in order to achieve a converged deformed state. The aeroelastic method has operated in parallel with 4 parallel processes. Figure 11 displays the computed static deformation for the entire F-16 fighter aircraft. The maximum positive and negative displacement in z-direction per deformation step is shown in Figure 12. The final maximum positive displacement (after the sixth deformation step) is 223.3 mm or $0.0647 l_{str}$.

In a code-to-code comparison with multi-block results (see Figure 12) it is observed that the computed results are in agreement with multi-block CFD results. A small difference in maximum upward displacement is observed which is due to differences in engine settings and grid resolution.



4 Conclusions

First experiences with an aeroelastic method for geometrically complex aircraft configurations having multiple components have been reported. The aeroelastic method has been employed for a high-lift wing in the linear range of the lift curve. The numerical results computed with the aeroelastic method have been verified for a generic fighter configuration. The aeroelastic method is fully automated. Due to application of unstructured CFD technology a short turnaround time for geometrically complex configurations with multiple components can be achieved.

For the high-lift wing it has been illustrated that besides a linear bending and associated torsion of the high-lift swept wing, local deformation of the control surfaces has been found. The results demonstrate the capability to assess the effect of aeroelastic deformation with respect to an already optimised rigid flap-gap. A structural model of a high-lift wing has been defined which models the individual high lift components and the attachments (tracks). Further improvements in the structural model can be foreseen, such as for example the application of a CSM model for the high-lift wind tunnel model.

The potential of the aeroelastic method for studying the aero-elastic behaviour of complex aircraft geometries with multiple components is large. Firstly, the results of the aeroelastic method will contribute to a better understanding of the Reynolds extrapolation process needed to extrapolate wind tunnel results to flight conditions. Similar deformation behaviour can be expected for a high-lift wing under flight-conditions due to differences in local stiffness of the various components. In particular the occurrence of flow separation or reattachment (e.g. near maximum lift on slat, flap or main wing) will have a local effect on the forces acting on the individual components.

Secondly, the aeroelastic method will enable to assess hinge loads on tracks more accurately and the aeroelastic method will give more insight in the complex physical flow phenomena occurring near maximum lift (in flight and in wind tunnel tests). Further research (e.g. flight tests) will be needed to discriminate the influence of aeroelastic effects for instance on high-lift performance, noise and hinge loads.

The study for the generic fighter illustrates as well that the aeroelastic characteristics of a fighter aircraft with a higher level of geometrical and structural detail, due to installation of weapons, pods and fuel tanks, can be examined in a relatively short turnaround time using unstructured CFD technology.



Acknowledgements

The authors wish to thank Jürgen Quest (ETW) for providing useful comments and feedback concerning the aeroelastic computations conducted for the high-lift wing reported in this paper.

5 References

- [1] Flight International, “Broken Mould”, pp. 28-31, January 25-31, 2005.
- [2] <http://www.luchtvaartnieuws.nl/news/?id=7353>, “Stork Aerospace belangrijke partner in productie Falcon 7X van Dassault”, February 15, 2005.
- [3] Kumar, A., Hefner, J.N., “Future challenges and opportunities in aerodynamics”, ICAS 2000 Congress, 2000.
- [4] Burg, J.W. van der, Maseland, J.E.J., Brandsma, F.J., “Low speed maximum lift and flow control”, Journal Aerospace Science and Technology, Elsevier, pp. 389-400, April, 2004
- [5] “Airbus targets the 7E7 niche with new plane design”, The Seattle Times, December 11, 2004.
- [6] “Structures”, Aerospace America, December 2004.
- [7] A review of aeronautics R&D at FAA and NASA, Hearing before the subcommittee on space and aeronautics committee on science house of representatives, One hundred eight congress, 85-418PS, 2003.
- [8] Galpin, S.A., Melin, T., “HELIX: Innovative high-lift aerodynamic concepts, an overview”, paper presented at the KATnet/GARTEUR High Lift Workshop, Stockholm, Sweden, September, 2002.
- [9] Willshire, B. “Quiet Technology Aircraft Program, Doing the Wright stuff: 100 years of aviation and the environment”, NASA, Office of Aero-space Technology, 2003.
- [10] “NASA comes to the aid of aircraft-noise sufferers”, Press release NASA Langley Research Center, August 2001.
- [11] TAURUS, “Technology development for aeroelastic simulations on unstructured grids”, Description of Work, Annex B to contract No. G4RD-CT2001-00403, September, 2000.
- [12] Eurolift II, European High Lift Programme II, Description of Work, Annex B to contract GRD-2004-502896, January, 2004.
- [13] Lokos W.A.; Bahm C.M.; Heinle, R.A., “Determination of stores pointing error due to wing flexibility under flight load”, Technical Memorandum TM 4646, NASA, 1995.
- [14] Prananta, B.B.; Tjatra, I.W.; Spekrijse, S.P.; Kok, J.C.; Meijer, J.J., “Static aeroelastic simulation of military aircraft configuration in transonic flow”, NLR Technical Publication 2001-346, August 2001.

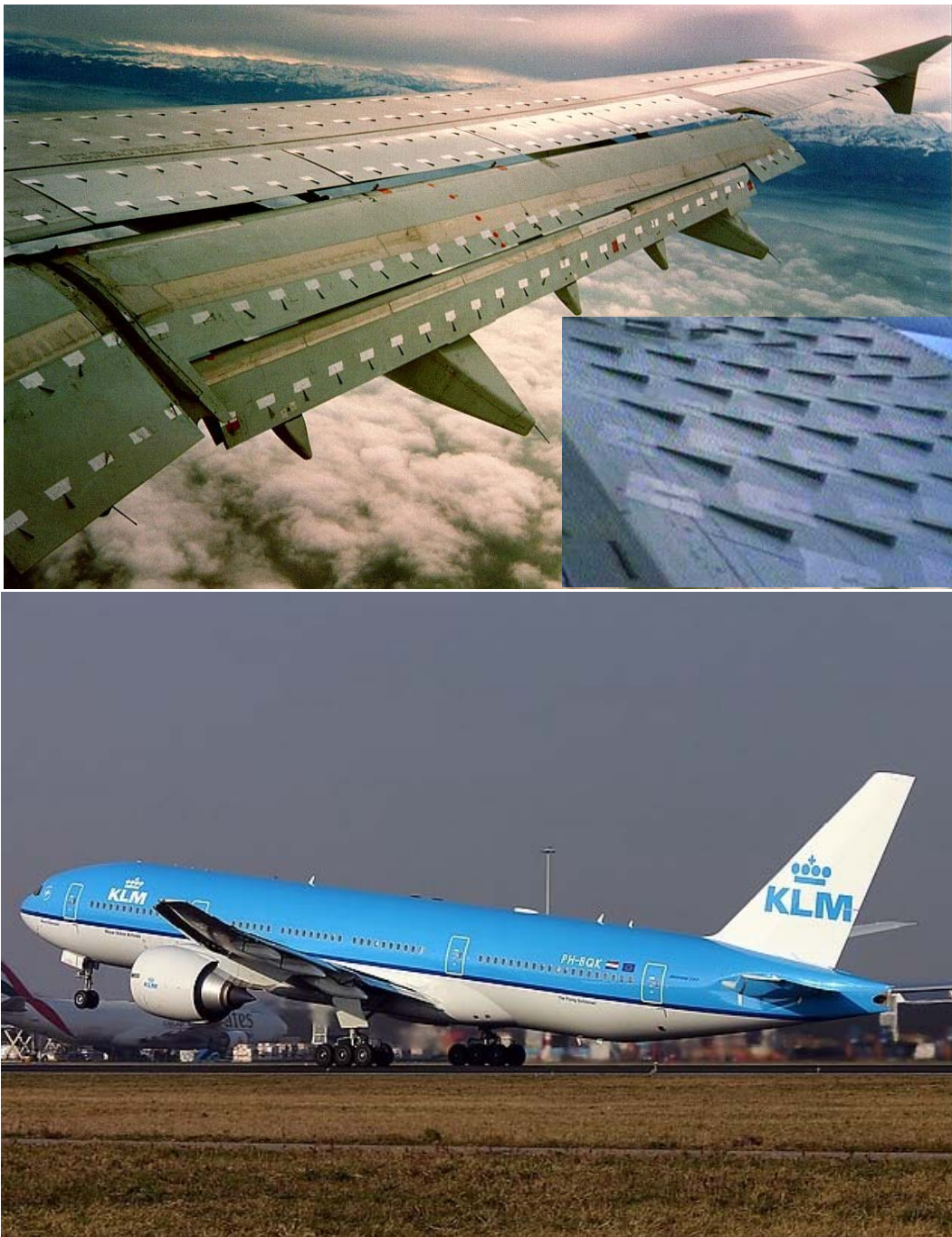


Figure 1 Example of in-flight high-lift wing instrumentation, where tufts are installed to verify e.g. flow separation (top). Aeroelastic bending of a Boeing 777 high-lift wing of commercial airliner KLM due to aerodynamic loads at take-off (bottom), copyright by Eric Meijer (Hoofddorp).

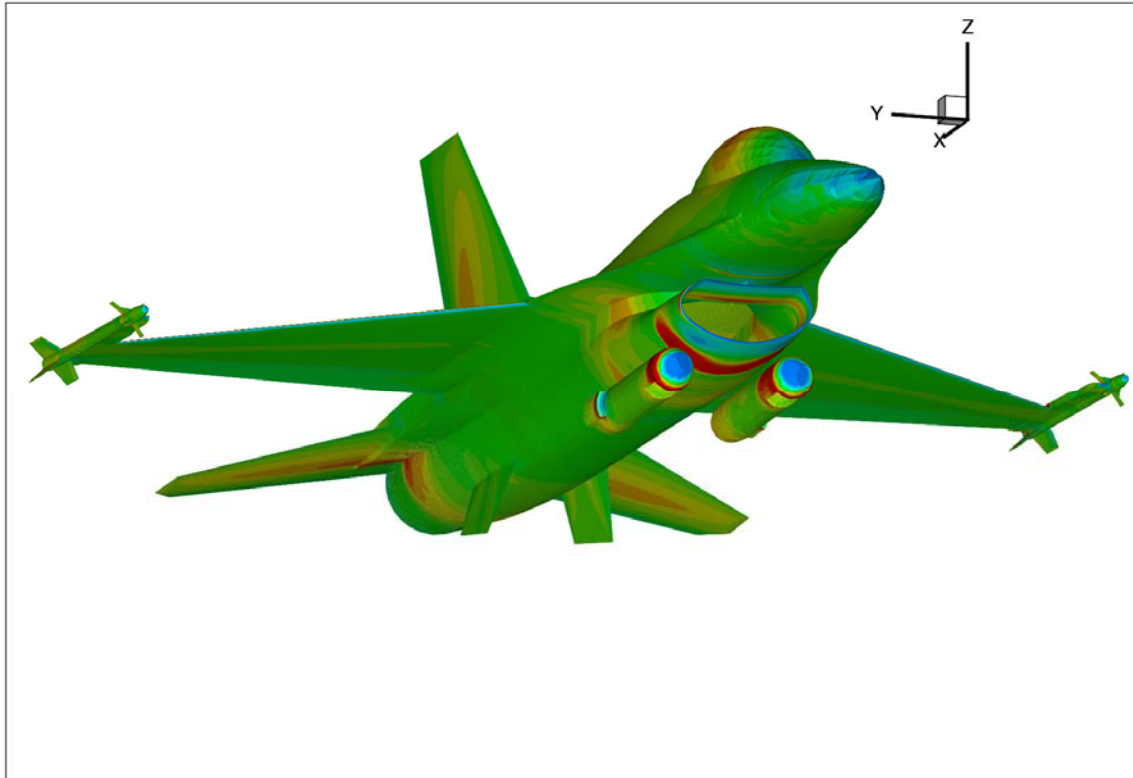


Figure 2 Example of a computed pressure distribution for a geometrically complex fighter configuration with an operational engine and recelite pods installed; Assessment of loads due to installation of recelite pods.

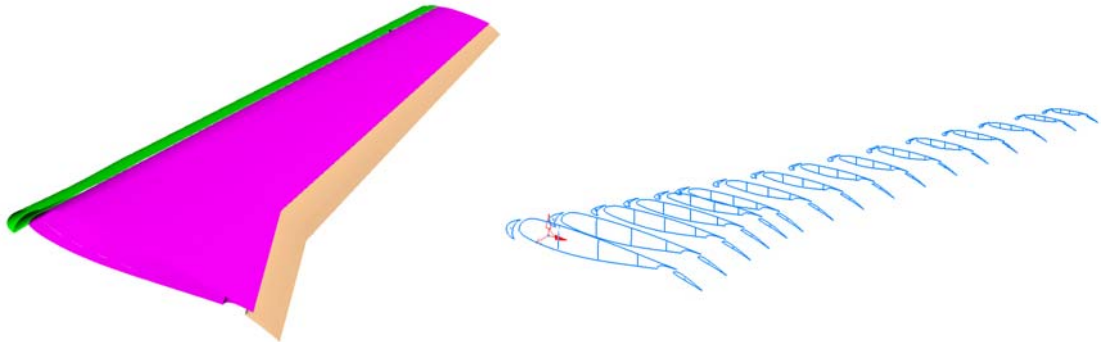


Figure 3 CFD geometry model of the high-lift wing of the KH3Y wind tunnel model with slat and flap deployed in take-off position (top). The fuselage is not shown. Geometrical representation of the high-lift wing in terms of 20 wing sections (bottom) needed for the derivation of the structural model.

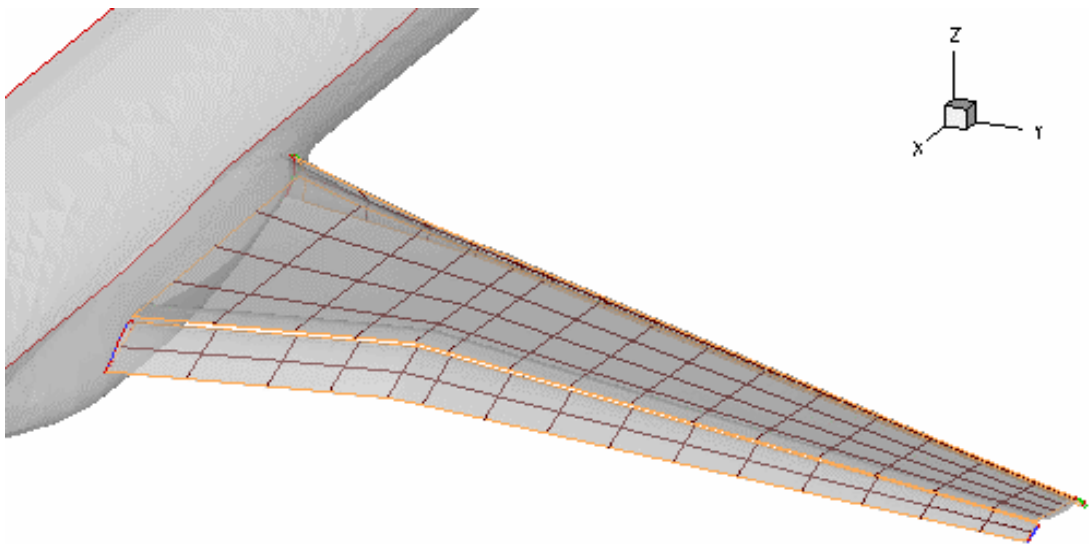


Figure 4 Structural model developed for the high-lift wing KH3Y wind tunnel model. The flap tracks and slat tracks have been modelled by requiring that structural nodes of the main wing and slat/flap have the same degrees of freedom. The slat is modelled by means of beam elements.

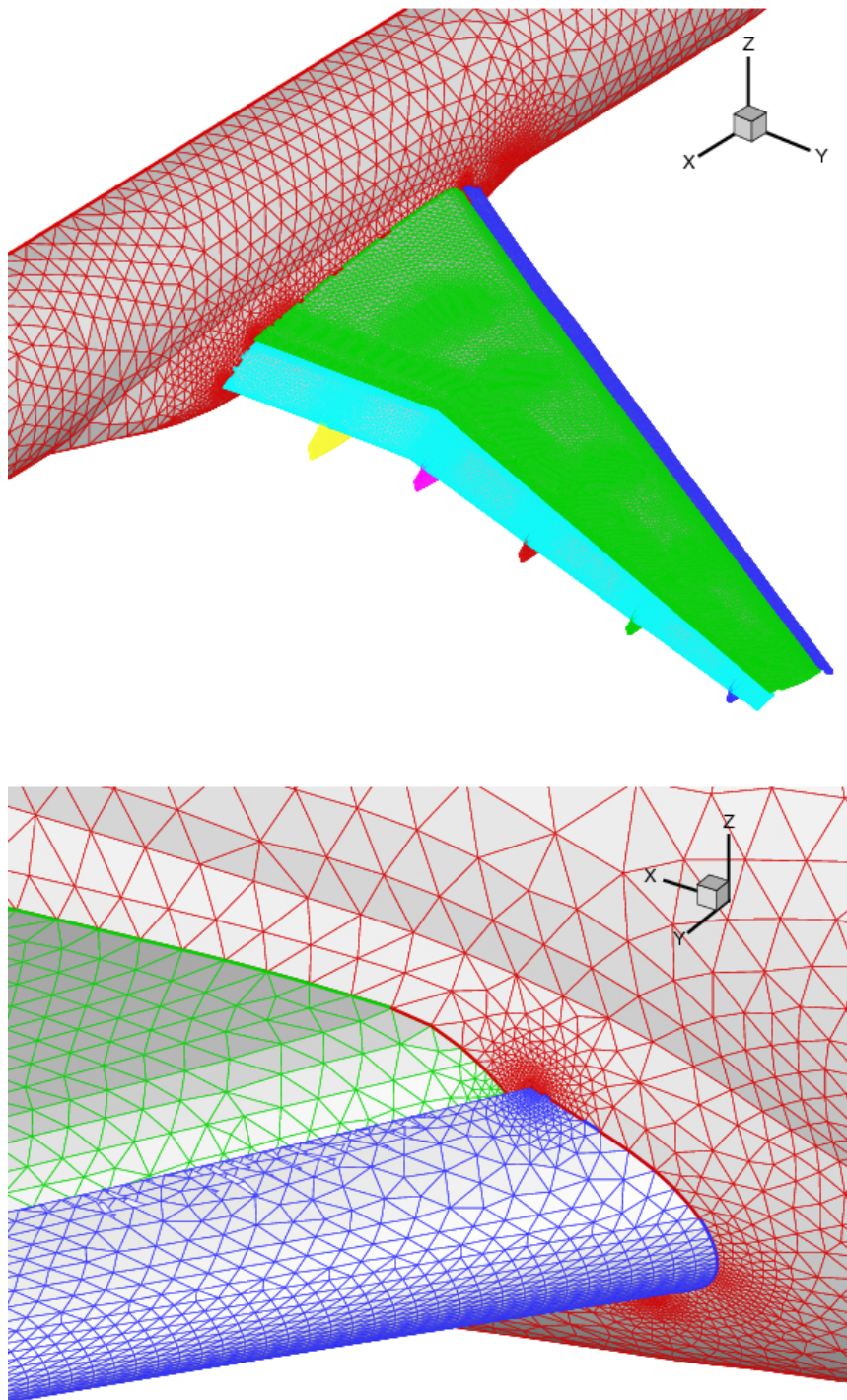


Figure 5 Computational surface grid for the high-lift wing with flap track fairings installed (the slat tracks have not been modelled in the aerodynamic grid). At the leading edges of the slat (blue), main wing (green) and flap (light blue) the grid is locally coarsened with a factor 4.

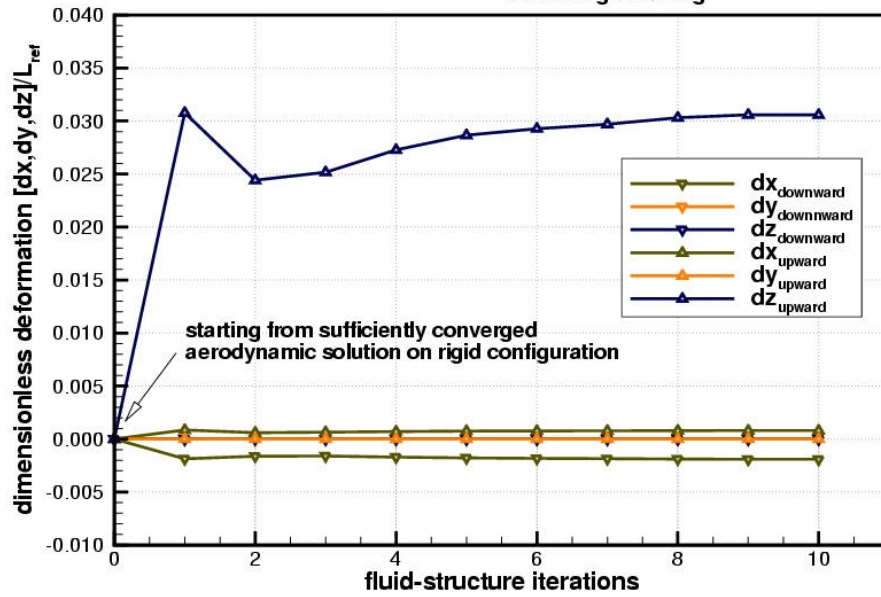


Figure 6 History of the aeroelastic computation for the high-lift configuration

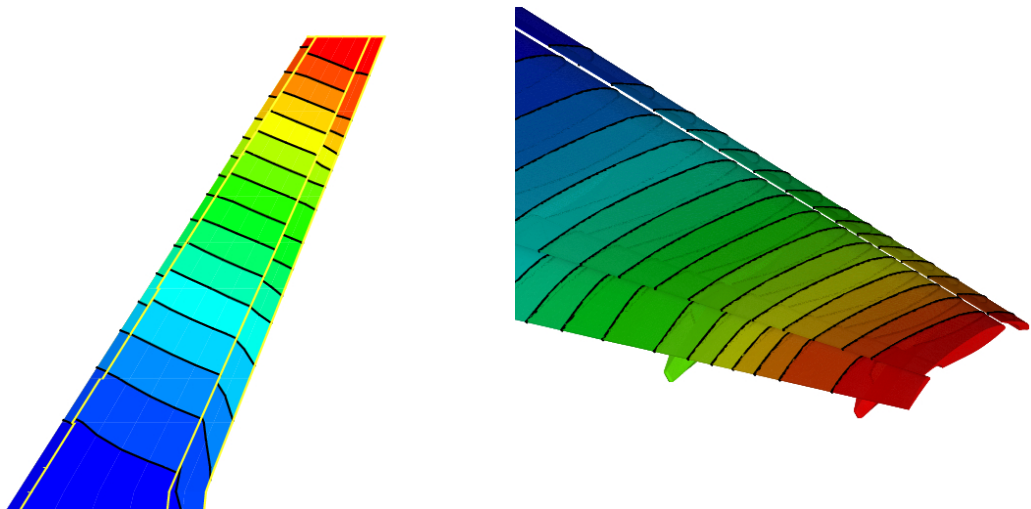


Figure 7 Computed deformation on the structural grid (left) and the computed deformed aerodynamic grid (right) of the high-lift wind tunnel model due to aerodynamic loading encountered in ETW. Contour lines with a same deflection in vertical (z-coordinate) direction are shown.

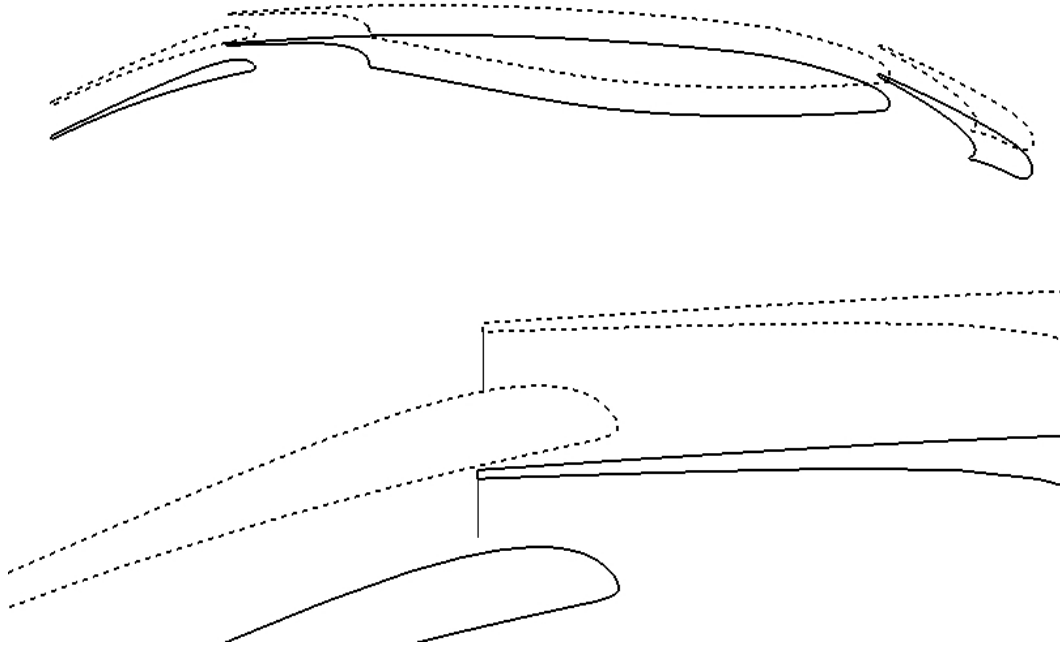


Figure 8 Derivation of the flap-gap height for the rigid (solid line) and the deformed (dashed line) high-lift wing. The computed flap-gap height for the aeroelastic deformed wing is projected onto the rigid case.

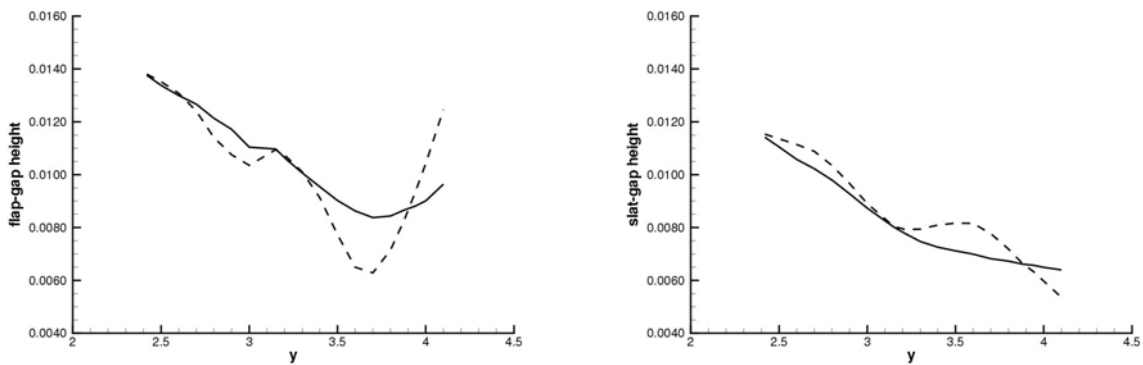


Figure 9 Computed height of the flap-gap (left) and slat-gap (right) for the rigid (solid line) and deformed (dashed line) high-lift wing between the third and fifth flap track fairing on the outer part of the high-lift wing. The flap-gap and slat gap height are scaled with the chord reference length l_{ref} .

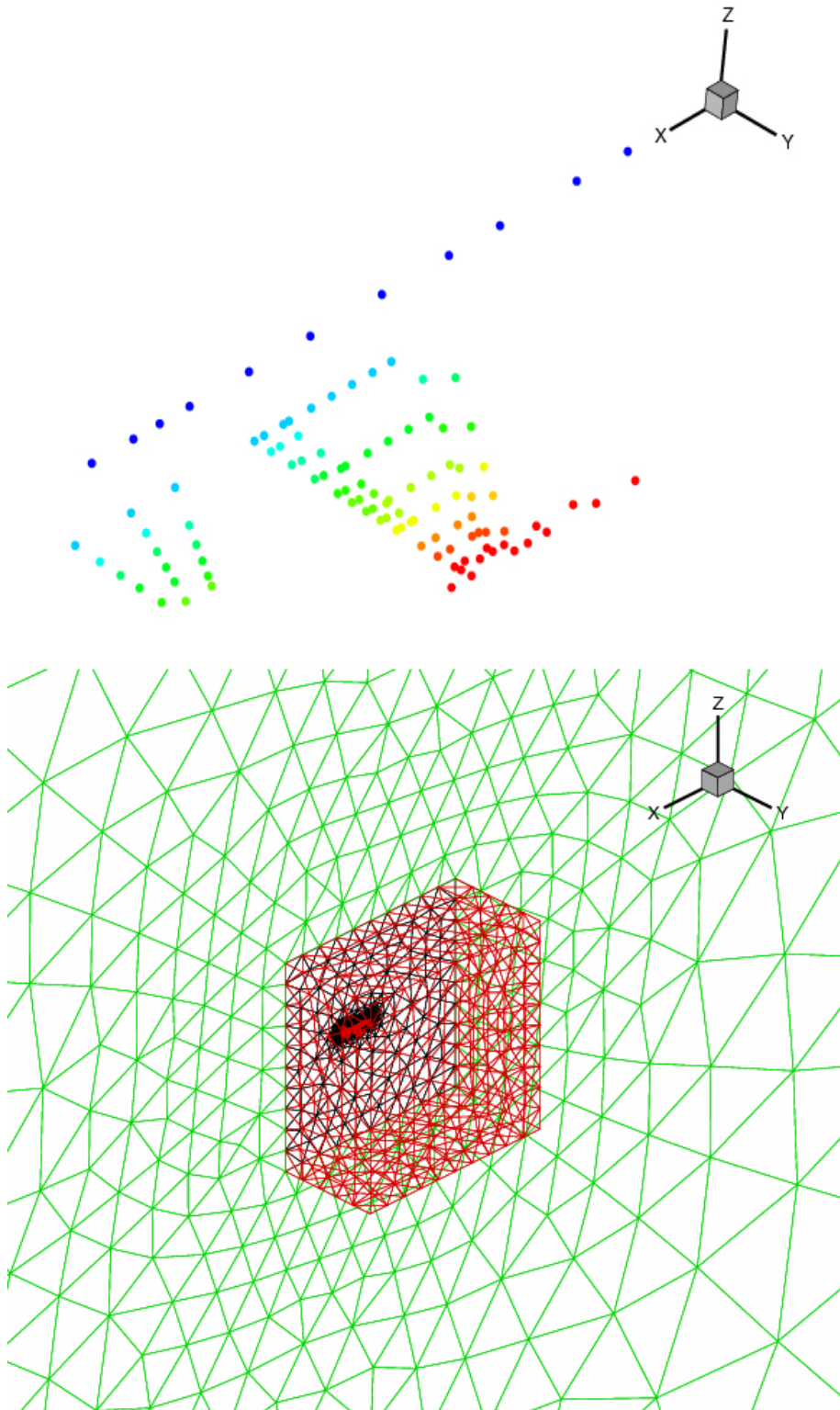


Figure 10 Structural nodes used for a generic fighter (top). Computational grid (bottom): symmetry plane (in green and black), an internal block boundary and the generic fighter (in red) are shown.

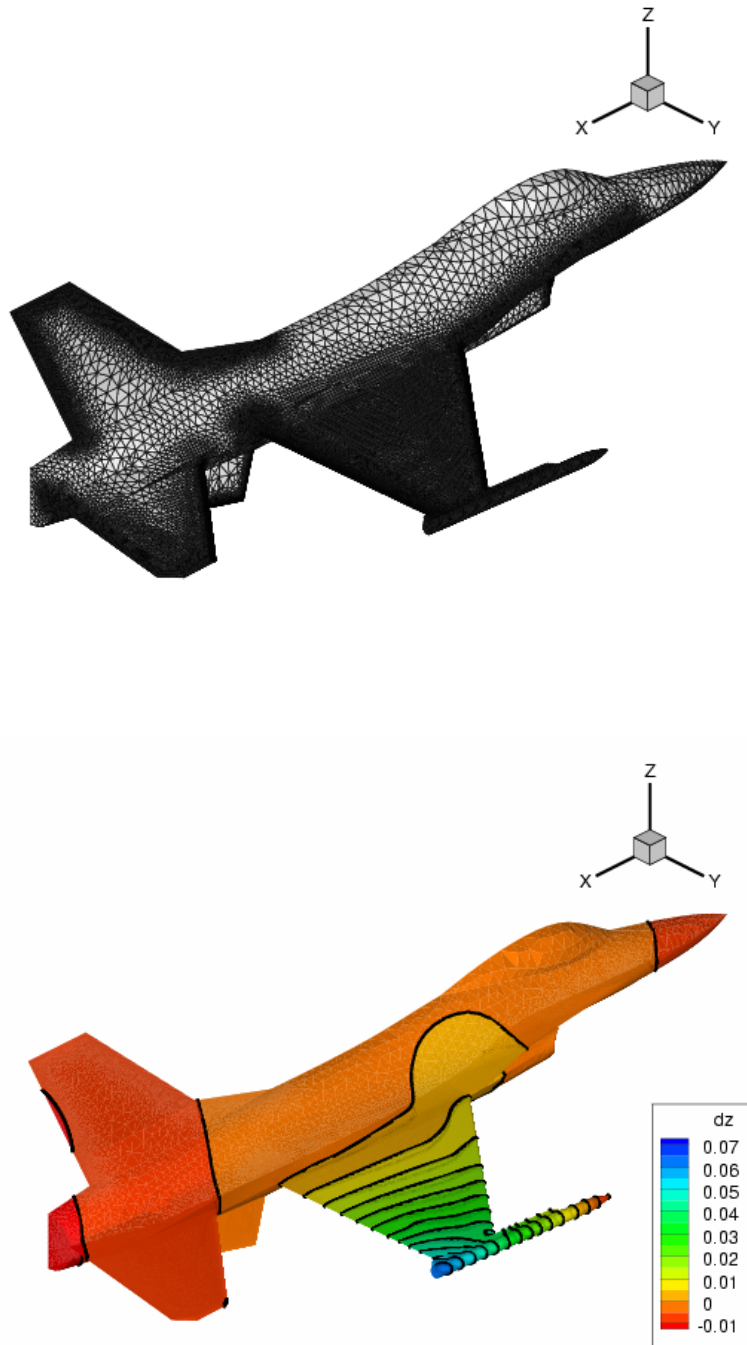


Figure 11 Aerodynamic surface grid for a generic fighter aircraft with tip missiles (left) and contours (right) of the final computed wing deformation for a symmetry pull-up ($n_z=5$) maneuver at $M_\infty=0.9$ for fixed lift.

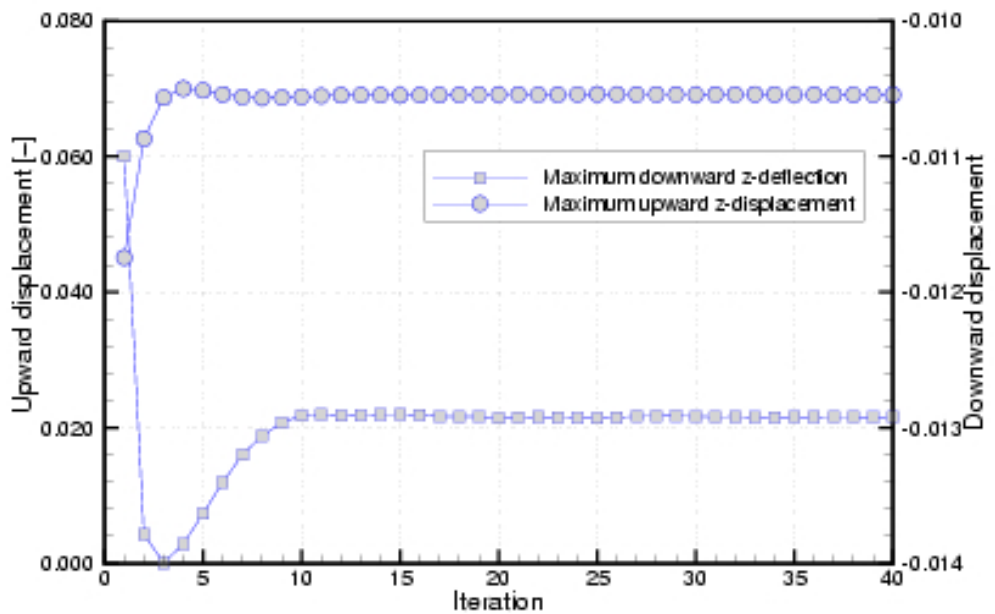
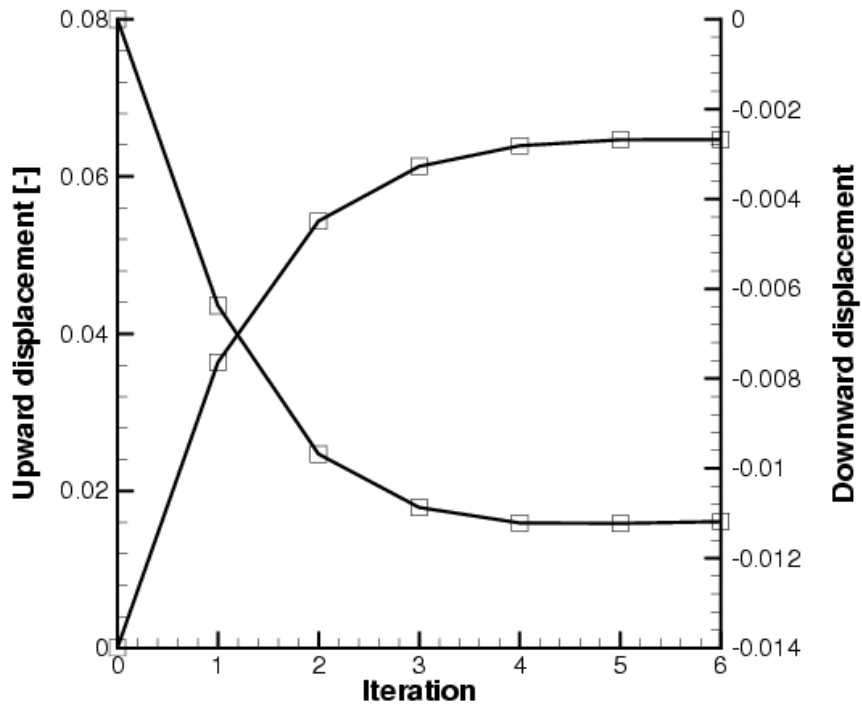


Figure 12 History of maximum positive and maximum negative deformation per aeroelastic deformation iteration is shown for a generic f16 fighter aircraft. A code-to-code comparison has been made between the unstructured result (left) and the multi-block ENFLOW result (right), see also Ref. [14].